High-frequency vortex response of anisotropic type-II superconductors

Chien-Jang Wu and Tseung-Yuen Tseng
Department of Electronics Engineering and Institute of Electronics, National Chiao-Tung University, Hsinchu, Taiwan, Republic of China

(Received 24 October 1995; revised manuscript received 1 February 1996)

The theory of the self-consistent treatment of vortex dynamics developed by Coffey and Clem is extended to the case of anisotropic type-II superconductors. The vortex response to a microwave electromagnetic field is theoretically investigated based on the associated complex rf magnetic permeability of anisotropic superconductors. Microwave dissipation due to vortex motion is studied as a function of the temperature, dc magnetic field, and microwave frequency. Comparisons of numerical results between anisotropic and isotropic superconductors are also given. The influence of the thin edge of superconducting platelets on the microwave properties is specifically examined as well. The extension presented provides the possible applicability in studying the high-frequency response of real anisotropic high-temperature superconducting single-crystal platelets in the mixed state. [S0163-1829(96)03725-3]

I. INTRODUCTION

Measurements of the vortex response to alternating magnetic fields or transport currents are commonly applied to investigate the vortex dynamics in type-II superconductors. At present, there exist many experimental techniques to probe the dissipation and screening such as the vibrating-reed resonator,[1,2] torsional oscillator,[3] ac magnetic permeability,[4] and microwave surface impedance.[5–8] All the ac measurements can be performed by superimposing a small ac field on a large dc field. A small ac field interacts with the penetrated vortices near the surface of the specimen and deforms the vortex lattice therein, which in turn propagates into the interior of the superconductor. The propagation is pushed forward through vortex interactions and slowed down by pinning and viscous drag forces. Accordingly, the dissipation and shielding properties of type-II superconductors are strongly dependent on the vortex dynamics. With related measurements, the models for the pinning and motion of vortices in the mixed state can be verified.[4,9–11]

In general, the ac response of superconductors in the mixed state includes linear and nonlinear responses. In the linear response, the induced current density is proportional to a small ac field and independent of the amplitude of the ac field. If the current density is related to the amplitude, one then speaks of a nonlinear response. In type-II superconductors, the existence of vortex pinning due to impurities will generally cause a nonlinear magnetic ac response above the threshold amplitude of the driving field.[11] The crossover from a linear to nonlinear response has been investigated from a unique macroscopic viewpoint by van der Beek *et al.* [12] The linear response in the regime of thermally assisted flux flow is better understood in terms of the resistive state[13–15] and London electrodynamics, whereas the Bean critical-state model is often used in the nonlinear regime.[16,17] In the thermally assisted flux flow (TAFF) phenomenology, the thermally activated depinning of the vortex lines is incorporated based on the extension of the Bardeen-Stephen (BS) flux flow model.[18] van der Beek and Kes[19] have successfully utilized the TAFF model to reproduce the irreversibility line (IL) for the vortex liquid. Their ac susceptibility has been theoretically described by a dislocation-mediated flux-creep approach, which includes elastic and plastic creeps. The plastic creep comes from the dislocation of the flux-line lattice (FLL), while elastic creep from elastic deformation of the FLL. In a small driving field, it is expected that the plastic creep will dominate. The high-frequency vortex response of high-temperature superconductors has also been studied based on the TAFF model reported by Yeh.[20] He considered a pinned Abrikosov FLL of a superconducting single crystal near the depinning threshold, and the microwave response was investigated. As discussed elsewhere, Koshelev and Vinokur[21] have calculated the Campbell penetration depth and surface resistance of a pinned vortex lattice within the framework of collective pinning theory.[21–23] A quite distinct model in discussing the linear ac response of the viscous flux-line liquid has recently been done by Chen and Marchetti.[24] To incorporate the vortex-vortex interaction together with the nonlocality effect, they used the hydrodynamic model[25] to describe the response of a flux liquid to an ac field. Because of the existence of the nonlocality arising from the viscous forces, two different penetration depths are introduced which closely relate to the amplitude of the ac penetrating field. The hydrodynamic model is in contrast with the TAFF model, where nonlocality is rarely taken into account and only one ac penetration depth dominates the response. The response in the mixed state dominated by the two penetration depths has also been considered based on the two-mode electrodynamics approach of Sonin *et al.*[26] Their two-mode approach encompasses the nonlocal effects arising from long-range intervortex interactions as well as the effects of FLL elasticity. More recently, Sonin and Traito[27] have further considered the influence of the Bean-Livingston barrier on the surface impedance of a type-II superconductor. The suppression of dissipation due to this barrier was predicted.

In addition to the above-described theoretical approaches, there are more treatments worthwhile mentioning. A more general analysis of the linear ac response incorporating the effects flux pinning, flux flow, and flux creep, together with

nonlocality in type-II superconductors, has been undertaken by Brandt[28] and Coffey and Clem,[29–34] respectively. Making use of a continuum method in the FLL, Brandt calculated the complex ac penetration depth, surface impedance, complex resistivity, and magnetic ac permeability. Accordingly, the ac response can be discussed. Based on a self-consistent treatment of vortex dynamics, Coffey and Clem undertook an exhaustive investigation of the theory of ac magnetic permeability and surface impedance to study the high-frequency linear response of superconductors. We are here only concerned with the Coffey-Clem model. Applications of this phenomenological model to high-temperature superconductors have been accomplished by many workers. Revenaz *et al.* [5] explained quantitatively the data of the surface resistance of their samples, the high-T_c $YBa_2Cu_3O_{7-x}$ (YBCO) (Y:123) films. Also, the parameters in the Coffey-Clem model such as the Labusch constant, pinning frequency, and activation energy can be experimentally determined. In the low-field and low-temperature regime, the model was used to extract the viscosity and Labusch constant, together with their dependence, on temperature by Pambinanchi *et al.*[8] In the work of Owliaei *et al.*,[7] the microwave surface resistance of YBCO films was also well described by this model. In the field-dependent surface resistance, a crossover from the pinning-dominated regime to flux-flow regime (viscous force dominated) was found. The crossover is a consequence of the suppression of the pinning force due to the magnetic field. A similar study on another typical high-T_c system, Bi:2212 [$Bi_2Sr_2CaCu_2O_8$ (BSCCO)], was also taken by Hanaguri *et al.* [35] The magnetic-field-dependent Labusch parameter in BSCCO single crystals was reported to be similar to the conventional superconductors.

The Coffey-Clem model is developed and suitable for isotropic superconductors. As far as high-T_c superconductors are concerned, the applicability in studying the ac, rf, or microwave response is restricted to the case of a perpendicular field configuration. In this configuration, the magnetic field is applied perpendicularly to the main flat surfaces of both films and single-crystal platelets; namely, the field is parallel to the c axis. The vortex dynamics in this configuration (vortices are parallel to the c axis) is often considered as nearly isotropic because of the smaller anisotropy in the ab plane. As discussed above,[5,7,8,35] all experiments were performed in this configuration. In order to avoid demagnetization fields in single-crystal platelets in a perpendicular configuration, many workers have also investigated the same problems with an alternative, the parallel field configuration.[6,36–38] In the parallel field, the vortices are parallel to the ab plane and the vortex motion is highly anisotropic. Hao and Clem[39] have theoretically studied the anisotropic viscous flux motion in low fields in this configuration. For the purpose of investigating the linear vortex response to ac fields in the anisotropic flux motion, the validity of Coffey-Clem model needs reconsideration or modification. Therefore, the extension from isotropic to anisotropic superconductors in this model appears to be of importance and interest.

Our purpose in this paper is to generalize the Coffey-Clem model to be suited in the anisotropic superconductors. The linear response based on our derivations will be systematically analyzed in the microwave regime specifically. The possible pronounced effects of thin edges of platelets (due to anisotropy) on microwave properties will be discussed detailedly as well. Our results are expected to be applicable to the study of the high-frequency response for high-T_c superconducting single-crystal platelets especially in the parallel field configuration.

II. MODEL OF VORTEX DYNAMICS AND ITS EXTENSION

We first briefly review the Coffey-Clem model,[29–34] namely, the self-consistent theory of vortex dynamics. The vortex dynamics is treated self-consistently by including the nonlocal effects arising from the coupling of the supercurrent and vortex displacements. Taking account of the response of the normal fluid, the two-fluid model in the presence of moving vortices is generalized. Creep effects are described in terms of the Brownian motion in a periodic potential; thereby a dynamical complex mobility is obtained. The electrodynamics of isotropic type-II superconductors is governed by the two-fluid equation, Ohm's law for a normal fluid, London equations, Ampère's and Faraday's laws, and the equation of motion for a vortex. The theory gives the complex ac penetration depth $\tilde{\lambda}$ as follows:[29]

$$\tilde{\lambda}(\omega,B_0,T)=\left[\frac{\lambda^2(B_0,T)-(i/2)\tilde{\delta}_{\rm vc}^2(B_0,T,\omega)}{1+2i\lambda^2(B_0,T)/\delta_{\rm nf}^2(B_0,T,\omega)}\right]^{1/2}, \quad (1)$$

where $\lambda(B_0,T)$ is the magnetic-field and temperature-dependent London penetration depth, $\delta_{\rm nf}$ is the normal-fluid skin depth defined as $\delta_{\rm nf}=(2\rho_{\rm nf}/\mu_0\omega)^{1/2}$. The $\tilde{\delta}_{\rm vc}$ in Eq. (1) is the effective skin depth due to creep and vortex motion and is expressed as $\tilde{\delta}_{\rm vc}=(2\tilde{\rho}_v/\mu_0\omega)^{1/2}$, with effective resistivity $\tilde{\rho}_v=B_0\phi_0\tilde{\mu}_v(\omega,B_0,T)$, and the dynamic mobility is given as

$$\tilde{\mu}_v(\omega,B_0,T)=\frac{1}{\eta}\left[1+\left(-\frac{i\omega\eta}{\alpha\kappa_p}+\frac{1}{I_0^2(\nu)-1}\right)^{-1}\right]^{-1}, \quad (2)$$

where η is the viscous drag constant, κ_p the Labusch constant, $\alpha=I_1(\nu)/I_0(\nu)$, I_1 and I_0 are the modified Bessel functions of the first kind, with argument $\nu=U_0(B,T)/2k_BT$, and U_0 is the activation barrier height of the potential. The flux quantum ϕ_0 and the static magnetic induction B_0 inside the superconductor are related via the intervortex spacing a_0 as $B_0\approx\phi_0/a_0^2$. Also, the assumptions of a_0 being much less than the sample dimension and much greater than the displacements of vortex motion have been made in advance. In the linear response theory, the displacements are typically less than 1 Å .[19,20] Coffey and Clem also calculated the complex penetration depth in the absence of flux creep, and their result is[31]

$$\tilde{\lambda}(\omega,B_0,T)=\left[\frac{\lambda^2(B_0,T)+[\lambda_c^{-2}(B_0,T)-2i\delta_f^{-2}(B_0,T,\omega)]^{-1}}{1-2i\lambda^2(B_0,T)/\delta_{\rm nf}^2(B_0,T,\omega)}\right]^{1/2}. \quad (3)$$

Here the pinning penetration depth[40] (Campbell penetration depth) λ_c and flux-flow penetration depth[41] δ_f are, respectively, defined by

$$\lambda_c^2 \equiv \frac{B_0\phi_0}{\mu_0\kappa_p}, \quad \delta_f^2 \equiv \frac{2B_0\phi_0}{\mu_0\eta\omega}. \tag{4}$$

Based on the key result, Eq. (1) or (3), the high-frequency response is able to be analyzed from the associated surface impedance or complex magnetic permeability according to the geometry to which one refers. For a semi-infinite superconductor, we study the response through the surface impedance $Z_s = R_s + iX_s$, given by[31]

$$Z_s = R_s + iX_s = i\omega\mu_0\tilde{\lambda}(\omega, B_0, T). \tag{5}$$

As for a slab with thickness $2c$ and right circular cylinder of radius c, the corresponding complex magnetic permeabilities are found to be[31]

$$\tilde{\mu}_{\text{slab}} = \frac{\tilde{\lambda}}{c}\tanh\left(\frac{c}{\tilde{\lambda}}\right), \tag{6}$$

and

$$\tilde{\mu}_{\text{cyl}} = \frac{2\tilde{\lambda}}{c}\frac{I_1(c/\tilde{\lambda})}{I_0(c/\tilde{\lambda})}, \tag{7}$$

respectively.

The surface impedance Z_s given in the Coffey-Clem model can be described well in terms of the circuit representation as analogous to the circuit representation of the traditional two-fluid model.[42] The supercarrier contribution to the impedance is represented by the kinetic inductor $l_s = \mu_0\lambda^2$, the flux pinning by an inductor $l_f = \phi_0 B_0/\kappa_p$ together with a damping resistor $\rho_f = \phi_0 B_0/\eta$, and the flux creep is represented by a creep resistor $\rho_c = \phi_0 B_0 \omega_c/\kappa_p$ in series with l_f. The crossover frequency ω_c is defined[5] as $\omega_c = \omega_0/[I_0^2(\nu)-1]^{1/2}$, with $\omega_0 = (\kappa_p/\eta)I_1(\nu)/I_0(\nu)$. The complete circuit representation of Z_s due to vortex dynamics can be seen in Ref. 42.

We now generalize the Coffey-Clem theory to anisotropic case. We consider a uniaxial anisotropic type-II superconductor in the shape of a long rectangular rod whose length, width, and thickness are $|z| \leqslant b$, $|x| \leqslant a$, and $|y| \leqslant c$, respectively. The superconductor has been cooled in a dc magnetic field parallel to the z axis, producing a uniform vortices lattice. The microwave field $\hat{\mathbf{z}}h_0 e^{-i\omega t}$ is applied parallel to the four planes at $x = \pm a$ and $y = \pm c$, and $\mu_0 h_0 \ll B_0$, the static field in the interior of superconductor. This arrangement is just the usual parallel field configuration in microwave technique such as in the cavity perturbation method.[6] Meanwhile, the sample dimensions are denoted as the crystallographic correspondences of high-T_c superconducting single-crystal platelets. The thickness is often prepared much less than the width. We assume that the dynamic properties in the ab plane are isotropic and the length of the rectangular rod is large enough that the demagnetizing field can be neglected. By matching the boundary conditions at $x = \pm a$ and $y = \pm c$, the field inside the sample induced by applying a microwave field can be calculated. The result is

$$\mathbf{B}(x,y,t) = \sum_{n=0}^{\infty}(-1)^n \frac{2\mu_0 h_0}{q_n}\left[\cos\left(\frac{q_n}{a}x\right)\frac{\cosh(k_y y)}{\cosh(k_y c)} + \cos\left(\frac{q_n}{c}y\right)\frac{\cosh(k_x x)}{\cosh(k_x a)}\right]e^{-i\omega t}. \tag{8}$$

Here k_x, k_y are expressed as

$$k_x^2 = \frac{1}{\tilde{\lambda}_c^2} + \frac{q_n^2}{c^2}\frac{\tilde{\lambda}_a^2}{\tilde{\lambda}_c^2} \tag{9}$$

and

$$k_y^2 = \frac{1}{\tilde{\lambda}_a^2} + \frac{q_n^2}{a^2}\frac{\tilde{\lambda}_c^2}{\tilde{\lambda}_a^2}, \tag{10}$$

where $q_n = (n+\frac{1}{2})\pi$, $n = 0,1,2,3,\ldots$. The $\tilde{\lambda}_a, \tilde{\lambda}_c$ are complex penetration depths in the a and c directions, being determined self-consistently. The total current density $\mathbf{J} = \hat{\mathbf{x}}J_x + \hat{\mathbf{y}}J_y$ can be directly calculated via Ampère law $\mathbf{J} = \mu_0^{-1}\nabla\times\mathbf{B}$; we have

$$J_x = J_{x0}\sum_{n=0}^{\infty}(-1)^n\left[\frac{c}{q_n}k_y\cos\left(\frac{q_n}{a}x\right)\frac{\sinh(k_y y)}{\cosh(k_y c)} - \sin\left(\frac{q_n}{c}y\right)\frac{\cosh(k_x x)}{\cosh(k_x a)}\right]e^{-i\omega t}, \tag{11}$$

$$J_y = J_{y0}\sum_{n=0}^{\infty}(-1)^n\left[\sin\left(\frac{q_n}{a}x\right)\frac{\cosh(k_y y)}{\cosh(k_y c)} - \frac{a}{q_n}k_x\cos\left(\frac{q_n}{x}y\right)\frac{\sinh(k_x x)}{\cosh(k_x a)}\right]e^{-i\omega t}, \tag{12}$$

where coefficients are $J_{x0} = 2h_0/c$ and $J_{y0} = 2h_0/a$. The electric field $\mathbf{E} = \hat{\mathbf{x}}E_x + \hat{\mathbf{y}}E_y$ is easily obtained by Faraday's law $\nabla\times\mathbf{E} = -\partial\mathbf{B}/\partial t$,

$$E_x = E_{x0}\sum_{n=0}^{\infty}(-1)^n\left[\frac{c}{q_n}k_y\cos\left(\frac{q_n}{a}x\right)\frac{\sinh(k_y y)}{\cosh(k_y c)} - \sin\left(\frac{q_n}{c}y\right)\frac{\cosh(k_x x)}{\cosh(k_x a)}\right]e^{-i\omega t}, \tag{13}$$

$$E_y = E_{y0}\sum_{n=0}^{\infty}(-1)^n\left[\sin\left(\frac{q_n}{a}x\right)\frac{\cosh(k_y y)}{\cosh(k_y c)} - \frac{a}{q_n}k_x\cos\left(\frac{q_n}{c}y\right)\frac{\sinh(k_x x)}{\cosh(k_x a)}\right]e^{-i\omega t}. \tag{14}$$

The E_{x0}, E_{y0} in Eqs. (13) and (14) are evaluated as

$$E_{x0} = \frac{i\omega\mu_0 2h_0 c(a^2k_x^2 + q_n^2)}{q_n^4 - a^2c^2k_x^2k_y^2} = -i\omega\mu_0\tilde{\lambda}_a^2\frac{2h_0}{c}, \tag{15}$$

$$E_{y0} = \frac{i\omega\mu_0 2h_0 a(c^2k_y^2 + q_n^2)}{q_n^4 - a^2c^2k_x^2k_y^2} = -i\omega\mu_0\tilde{\lambda}_c^2\frac{2h_0}{a}. \tag{16}$$

The corresponding normal-fluid current density $\mathbf{J}_n$ is given straightforwardly through the Ohmic relation

$\mathbf{J}_n=\hat{\mathbf{x}}J_{nx}+\hat{\mathbf{y}}J_{ny}=\vec{\boldsymbol{\sigma}}_{\rm nf}\mathbf{E}$, with $J_{nx}=\sigma_{\rm nfx}E_x$ and $J_{ny}=\sigma_{\rm nfy}E_y$. Here we have assumed that the resistivity tensor $\vec{\boldsymbol{\sigma}}_{\rm nf}$ is diagonal with entities $\sigma_{\rm nfx}$ and $\sigma_{\rm nfy}$ along the x and y directions, respectively.

The induced microwave current density in Eqs. (11) and (12) generates a Lorentz force acting on the vortices to oscillate back and forth near the surfaces of sample. The oscillation, in turn, propagates into the interior of superconductor, which is impeded by viscous drag friction together with a restoring force. The governed equation for vortex motion in anisotropic superconductor is

$$\vec{\boldsymbol{\eta}}\,\dot{\mathbf{u}}+\vec{\boldsymbol{\kappa}}_p\mathbf{u}=\mathbf{J}\times\phi_0\hat{\mathbf{z}}, \tag{17}$$

where $\vec{\boldsymbol{\eta}}$ is the viscosity tensor in the absence of creep with diagonal elements η_x and η_y, $\vec{\boldsymbol{\kappa}}_p$ the tensor of the restoring force constant with components κ_{px} and κ_{py}, and $\mathbf{u}$ the small vortex displacement deviating from its pinning site. By letting $\mathbf{u}=\hat{\mathbf{x}}u_x(x,y,t)+\hat{\mathbf{y}}u_y(x,y,t)=\hat{\mathbf{x}}u_{x0}f(x,y)e^{-i\omega t}+\hat{\mathbf{y}}u_{y0}g(x,y)e^{-i\omega t}$ and substituting it along with Eqs. (11) and (12) into Eq. (17), we have

$$u_x=u_{x0}\sum_{n=0}^{\infty}(-1)^n\left[\sin\left(\frac{q_n}{a}x\right)\frac{\cosh(k_y y)}{\cosh(k_y c)}-\frac{a}{q_n}k_x\cos\left(\frac{q_n}{c}y\right)\frac{\sinh(k_x x)}{\cosh(k_x a)}\right]e^{-i\omega t} \tag{18}$$

and

$$u_y=u_{y0}\sum_{n=0}^{\infty}(-1)^n\left[\frac{c}{q_n}k_y\cos\left(\frac{q_n}{a}x\right)\frac{\sinh(k_y y)}{\cosh(k_y c)}-\sin\left(\frac{q_n}{c}y\right)\frac{\cosh(k_x x)}{\cosh(k_x a)}\right]e^{-i\omega t}, \tag{19}$$

where u_{x0} and u_{y0} are given by $u_{x0}=\phi_0 J_{y0}/(-i\omega\eta_x+\kappa_{px})$ and $u_{y0}=\phi_0 J_{x0}/(-i\omega\eta_y+\kappa_{py})$.

The moving vortices generate a local magnetic flux density $\mathbf{B}_v=-\nabla\times(\mathbf{B}_0\times\mathbf{u})$, which will redistribute the current density. The nonlocal effect due to vortex motion manifests itself in the modified London equation

$$\nabla\times(\vec{\boldsymbol{\Lambda}}\mathbf{J}_s)=-(\mathbf{B}-\mathbf{B}_v). \tag{20}$$

Here the tensor $\vec{\boldsymbol{\Lambda}}$ contains the information on the anisotropic field-dependent London penetration depths in the a and c directions, λ_a and λ_c; the entities are $\mu_0\lambda_a^2$ and $\mu_0\lambda_c^2$, while $\mathbf{J}_s$, the supercurrent density, is denoted as $\mathbf{J}_s=\hat{x}J_{sx}+\hat{y}J_{sy}$. Making use of Eqs. (8), (18), and (19), we can obtain the supercurrent density components J_{sx} and J_{sy} on the basis of Eq. (20). After a lengthy calculation, we have

$$J_{sx}=J_{sx0}\sum_{n=0}^{\infty}(-1)^n\left[\frac{c}{q_n}k_y\cos\left(\frac{q_n}{a}x\right)\frac{\sinh(k_y y)}{\cosh(k_y t)}-\sin\left(\frac{q_n}{c}y\right)\frac{\cosh(k_x x)}{\cosh(k_x a)}\right]e^{-i\omega t}, \tag{21}$$

$$J_{sy}=J_{sy0}\sum_{n=0}^{\infty}(-1)^n\left[\sin\left(\frac{q_n}{a}x\right)\frac{\cosh(k_y y)}{\cosh(k_y c)}-\frac{a}{q_n}k_x\cos\left(\frac{q_n}{c}y\right)\frac{\sinh(k_x x)}{\cosh(k_x a)}\right]e^{-j\omega t}, \tag{22}$$

where the coefficients are found as

$$J_{sx0}=\frac{1}{\mu_0\lambda_a^2}\left[\frac{2\mu_0 h_0\tilde{\lambda}_a^2}{c}+B_0u_{y0}\right],$$

$$J_{sy0}=\frac{1}{\mu_0\lambda_c^2}\left[\frac{2\mu_0 h_0\tilde{\lambda}_c^2}{a}+B_0u_{x0}\right].$$

The main anisotropic complex penetration depths $\tilde{\lambda}_a$ and $\tilde{\lambda}_c$, including all the physics of vortex dynamics due to microwave field, can then be obtained on the basis of the two-fluid equation $\mathbf{J}=\mathbf{J}_n+\mathbf{J}_s$. Evaluation of the x component of the current density yields

$$\tilde{\lambda}_a=\left[\frac{\lambda_a^2+(\lambda_{cx}^{-2}-2i\,\delta_{fx}^{-2})^{-1}}{1-2i\lambda_a^2/\delta_{\rm nfy}^2}\right]^{1/2}, \tag{23}$$

where we define

$$\lambda_{cx}^2\equiv\frac{B_0\phi_0}{\mu_0\kappa_{py}},\quad \delta_{fx}^2\equiv\frac{2\phi_0 B_0}{\mu_0\omega\eta_y},\quad \delta_{\rm nfy}^2\equiv\frac{2}{\mu_0\omega\sigma_{\rm nfx}}. \tag{24}$$

Similarly, consideration of the y component of the current density gives

$$\tilde{\lambda}_c=\left[\frac{\lambda_c^2+(\lambda_{cy}^{-2}-2i\,\delta_{fy}^{-2})^{-1}}{1-2i\lambda_c^2/\delta_{\rm nfx}^2}\right]^{1/2}. \tag{25}$$

Here we use the definitions

$$\lambda_{cy}^2=\frac{B_0\phi_0}{\mu_0\kappa_{px}},\quad \delta_{fy}^2=\frac{2\phi_0 B_0}{\mu_0\omega\eta_x},\quad \delta_{\rm nfx}^2=\frac{2}{\mu_0\omega\delta_{\rm nfy}}. \tag{26}$$

The similarity between Eqs. (23), (25), and (3) appears to be stimulated. However, some care should be taken in comparing these three equations. The complex penetration depth in the x direction, $\tilde{\lambda}_a$, is dependent on the restoring constant κ_{py}, viscous coefficient η_y, normal-fluid conductivity $\sigma_{\rm nfx}$, and London penetration depth λ_a, whereas $\tilde{\lambda}_c$ is on κ_{px}, η_x, $\sigma_{\rm nfy}$, and λ_c. These dependences elucidate the basic features of anisotropic vortex motion and can be regarded as rules for transforming Eq. (3) to Eqs. (23) and (25).

The above derivations are accomplished under the consideration of no creep effect. In the case where the creep is included, the corresponding anisotropic complex penetration depths $\tilde{\lambda}_a$ and $\tilde{\lambda}_c$ are easily produced according to the results of Coffey and Clem, Eqs. (1), (2), as well as the transformation rules described above. For example, if one makes some replacements in Eq. (1) with $\lambda\to\lambda_a$, $\delta_{\rm nf}\to\delta_{\rm nfy}$, $\tilde{\delta}_{\rm vc}\to\tilde{\delta}_{\rm vcy}$ and Eq. (2), $\eta\to\eta_y$, $\kappa_p\to\kappa_{py}$, a similar expression in Eq. (1) for $\tilde{\lambda}_a$ is readily obtainable. Similar substitutions in Eqs. (1) and (2) lead to $\tilde{\lambda}_c$.

Having obtained explicit forms of the anisotropic complex penetration depths given in Eqs. (23) and (25), the mi-

crowave response in the mixed state is therefore readily investigated from the relevant effective magnetic permeability. The associated magnetic permeability μ for a rectangular rod is $\mu=\langle B(x,y)\rangle/\mu_0 h_0$, where $\langle B(x,y)\rangle = (2a\times 2c)^{-1}\int_{-c}^{c}\int_{-a}^{a} B(x,y)dxdy$. Using the spatial part in Eq. (8) to evaluate the integration, we find

$$\mu=\sum_{n=0}^{\infty}\frac{2}{(n+\frac{1}{2})^2\pi^2}\left[\frac{\tanh(k_y c)}{k_y c}+\frac{\tanh(k_x a)}{k_x a}\right]. \quad (27)$$

Before performing the numerical calculations, we wish to illustrate some special considerations to reflect the generality of our results. In theoretical studies, one usually considers a slab geometry with thickness $2c$, namely, $2a\to\infty$. Then the permeability in Eq. (27) becomes

$$\mu=\frac{\tilde{\lambda}_a}{c}\tanh\left(\frac{c}{\tilde{\lambda}_a}\right), \quad (28)$$

which further reduces exactly to Eq. (6) if the slab is isotropic. Moreover, Eq. (28) reveals that the permeability of an anisotropic slab is clearly dependent on $\tilde{\lambda}_a$ instead of $\tilde{\lambda}_c$. This is a consequence of the anisotropic property also shown in the Meissner-state response from a conventional two-fluid model[43] and in the normal-state response.[6] By the way, in simplifying Eq. (27) to Eq. (28), the identity

$$\sum_{n=\text{odd}}\frac{1}{n^2}=\frac{\pi^2}{8}$$

has been used implicitly. If the rectangular rod considered here is an isotropic superconductor, then the permeability, in Eq. (27), reduces to

$$\mu=\sum_{n=0}^{\infty}\frac{2}{(n+\frac{1}{2})^2\pi^2}\left[\frac{\tanh(k'_y c)}{k'_{yc}}+\frac{\tanh(k'_x a)}{k'_x a}\right], \quad (29)$$

where $k'_x=(\tilde{\lambda}^{-2}+q_n^2 c^{-2})^{1/2}$ and $k'_y=(\tilde{\lambda}^{-2}+q_n^2 a^{-2})^{1/2}$. Expression (29) is not the same as that of Coffey and Clem; see Ref. 31 [Eq. (B8)]. Their permeability of an isotropic rectangular rod is rewritten, in our notation, as

$$\mu=\frac{\tilde{\lambda}}{c}\tanh\left(\frac{c}{\tilde{\lambda}}\right)+\sum_{n=0}^{\infty}\frac{2}{(n+\frac{1}{2})^2\pi^2}\frac{\tanh(k'_x a)}{{k'_x}^3\tilde{\lambda}^2 a}. \quad (30)$$

The primary distinction between Eqs. (29) and (30) lies in the different boundary conditions considered in finding the magnetic induction. The boundary conditions used in the paper of Coffey and Clem[31] are the continuity of magnetic induction only at two planes $x=\pm a$ and the reduction to those for a slab as $a\to\infty$. Our considerations here, however, are the continuity conditions of four planes at $x=\pm a$ and $y=\pm c$. It is thus evident that our result in expression (29) seems more relevant to the study of the microwave response in the parallel field configurations. Our results given in Eq. (27) for anisotropic superconductors and Eq. (29) for the isotropic one will be applied to investigate the vortex response together with the effects of the edges of thin platelets. For related permeabilities derived from a diffusion-type equation in the Meissner and normal states, we mention the papers of Wu and Tseng[44] and Gough and Exon.[6]

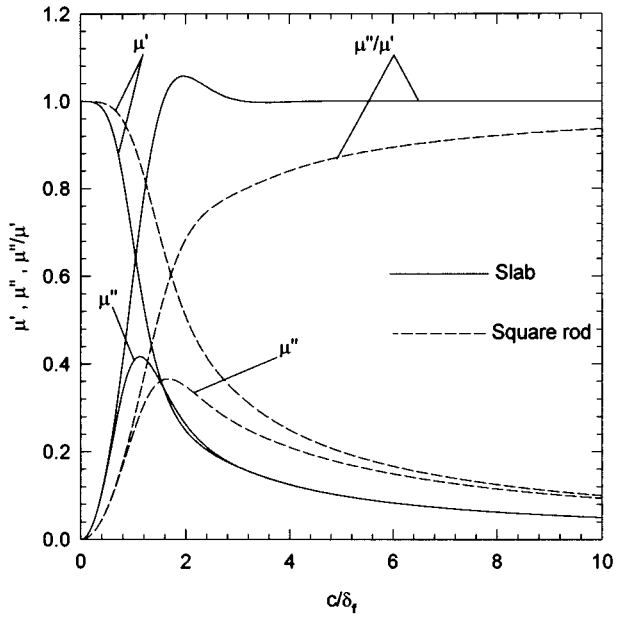

FIG. 1. Plot of permeabilities in Eqs. (29) and (6) as a function of c/δ_f, in the regime of flux-flow dynamics, where $\tilde{\lambda}=(1+i)\delta_f/2$ and δ_f is flux-flow penetration depth defined as $\delta_f^2=2B_0\phi_0/\mu_0\omega$. Here c is the half-thickness of the slab.

III. RESULTS AND DISCUSSION

We now demonstrate some numerical results and discuss those significant physics about the various vortex responses to a microwave field. The first case we consider is the isotropic superconducting rod whose complex permeability is given in Eq. (29). For simplicity, it is instructive to study the vortex dynamics dominated by flux flow. That is, the normal fluid is neglected and the complex penetration depth in Eq. (3) becomes $\tilde{\lambda}=(1+i)\delta_f/2$. Rearrangement of Eq. (29) as a function of a/δ_f and c/δ_f reveals that $\mu=\mu'+i\mu''$ has a minimum peak height (0.366) in the imaginary part μ'' when $a/\delta_f=c/\delta_f$, the square rod. In the extreme case $a\to\infty$, the slab has, however, a maximum peak in value of 0.417 in μ''. The results of μ'', μ', and μ''/μ' as a function of c/δ_f for these two special geometries are plotted in Fig. 1. The imaginary part μ'' conveys the microwave loss of dissipation, which is of vital importance in the analysis of the microwave response, whereas the real part μ' indicates the flux screening. As can be seen in Fig. 1, the dissipation is related to the sample dimensions. In slab geometry, the position of the dissipation peak occurs at $c/\delta_f=1.13$, while the square rod at $c/\delta_f=1.67$, a consequence of the skin size effect. In other words, the corresponding peak frequency of the square rod is greater than the slab. As a matter of fact, the peak frequency in the slab is the lowest and its corresponding peak height is, however, a maximum. The results clearly elucidate the dependence of microwave properties on geometry even in the isotropic superconductors. The linear response in the regime of flux flow is in fact nothing less than the resistive response (Ohmic response) or the TAFF response.[6,14,15] Also, if one wishes to investigate the irreversibility line[15,19] in the mixed states, the results here suggest some correlation with the geometry considered.

We go on to study the response of isotropic supercon-

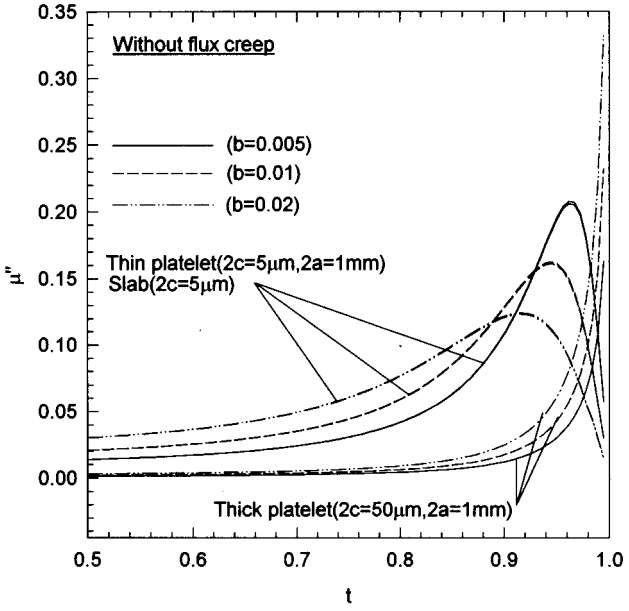

FIG. 2. Imaginary parts of permeabilities in Eq. (29) of a platelet and (6) of a slab as a function of reduced temperature $t \equiv T/T_c$ for a fixed frequency 10 GHz at various reduced fields $b \equiv B_0/B_{c_2}(0) = 0.005$, 0.1, and 0.2. The complex penetration depth $\tilde{\lambda}$ in Eq. (3) is used in the case without flux creep. The thickness of the slab is $2c = 5$ μm and the thick platelet has a width $2a = 1$ mm, thickness $2c = 50$ μm, while the thin platelet has $2a = 1$ mm and $2c = 5$ μm. The material constants used are given in the text.

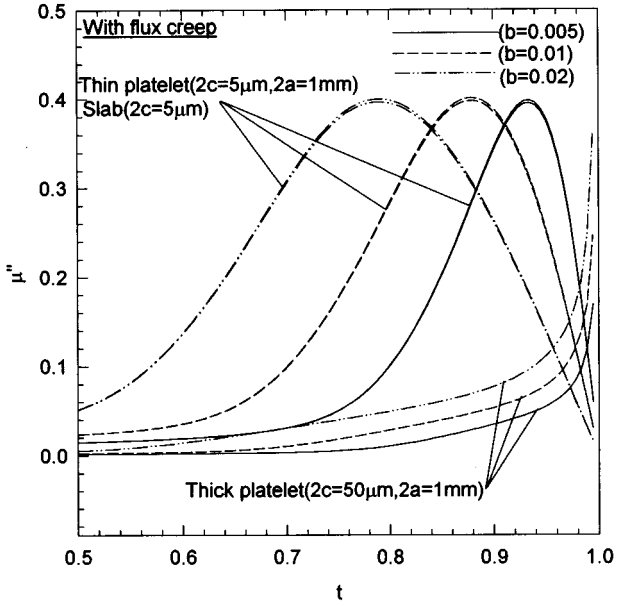

FIG. 3. Imaginary part of permeabilities in Eq. (29) of a platelet and (6) of a slab, as a function of reduced temperature $t \equiv T/T_c$ for a fixed frequency 10 GHz at various reduced fields $b \equiv B_0/B_{c_2}(0) = 0.005$, 0.1, and 0.2. The complex penetration depth $\tilde{\lambda}$ in Eq. (1) is used in the case with flux creep. The thickness of the slab is $2c = 5$ μm and the thick platelet has a width $2a = 1$ mm, thickness $2c = 50$ μm, while the thin platelet has $2a = 1$ mm and $2c = 5$ μm. The material constants used are given in the text.

ductors based on Eqs. (29), (6), (3), and (1). To numerically illustrate the dissipation as a function of temperature, magnetic field, and microwave frequency, we will use the parameters on the order of those for the familiar high-T_c system YBCO. However, we do not simulate the response for a specific sample. The parameters used in the study of Coffey and Clem[31] are reused at present. These are $\lambda = \lambda(0)[1-(T/T_c)^4]^{-1/2}\{1-[B_0/B_{c_2}(T)]\}^{-1/2}$, $\delta_f^2(B_0,T,\omega) = 2\rho_n(T)B_0/[\mu_0\omega B_{c_2}(T)]$, and $\delta_{\rm nf}^2(B_0,T,\omega) = \delta_n^2/f(B_0,T)$, where $\lambda(0) = 1400$ Å, $T_c = 91$ K, $B_{c_2}(T) = B_{c_2}(0)[1-(T/T_c)^2][1+(T/T_c)^2]^{-1}$, $\rho_n(T) = 1.1\times10^{-8}T + 2\times10^{-6}$ Ωm, $f(B_0,T) = 1-[1-(T/T_c)^4]\times\{1-[B_0/B_{c_2}(T)]\}$, and $B_{c_2}(0) = 112T$. The Labusch constant is $\kappa_p = \kappa_{p0}[1-(T/T_{c_2})^2]^2$, $\kappa_{p0} = 2.1\times10^4$ N m^{-2}, and activation barrier height $U_0 = U[1-(T/T_{c_2})]^{3/2}B_0^{-1}$, where $U = 0.15$ eV$-T$ and T_{c_2} is temperature at which $B_0 = B_{c_2}(T)$. Also we define reduced field $b \equiv B_0/B_{c_2}(0)$. Figure 2 shows the imaginary parts of permeabilities as a function of reduced temperature $t \equiv T/T_c$, at various reduced fields at fixed 10 GHz, for the three different geometries considered. These results are plotted from Eqs. (29), (6), and (3). It is interesting to observe that the dissipation peak near T_c disappears in the thick platelet (width = 1 mm, thickness = 50 μm), and the loss decreases sharply near T_c and to zero. The overall behaviors of the slab (thickness = 5 μm) and thin platelet (thickness = 5 μm, width = 1 mm) have essentially nothing different. The dissipation peaks are present, and losses are enhanced as a whole except at temperature very near T_c. The effects of a static (reduced) magnetic field, on the other hand, are illustrated in Fig. 2, too. By increasing the reduced field, the peak shape is broadened and the peak height is lowered for the slab or thin platelet. As for the thick platelet, the increase in field will greatly increase the loss, especially at a temperature just below T_c. The results shown in Fig. 2 are obtained under the consideration of no-flux creep effect. In the case where creep is included [Eq. (1)], the corresponding results are depicted in Fig. 3. Obviously, the inclusion of flux creep has prominently increased the dissipation μ''; see the scale. In the meantime, the effects of the magnetic field have some notable differences from those shown in Fig. 2. The peak broadens more when the field increases, while the height essentially does not decrease appreciably. Also, the temperature at the peak moves lower as compared with Fig. 2. From the results of Figs. 2 and 3, we deduce that whether the creep is considered or not, the microwave properties of thin platelets can be simply described by a slab with the same thickness, whereas in the thick plate, care should be taken. That is, in microwave studies of isotropic superconducting thin platelets, the effect of thin edges is usually negligible. In Fig. 4, the relation of μ'' vs t is again plotted at distinct frequencies at $b = 0.01$ for a slab (thickness = 5 μm). There, the solid lines indicate the results of flux creep [Eq. (1)], while dashed lines the results without creep [Eq. (3)]. The flux creep has a salient influence on μ'' specifically at frequencies of 1 and 10 GHz. At higher frequencies the μ'' is, however, very weakly affected. These phenomena are due to the fact that the creep is detected at low frequency.[5,12] At frequency $f < f_c = \omega_c/2\pi$, where ω_c is the flux-creep crossover frequency described earlier, the vortex dynamics is dominated by thermally activated flux creep

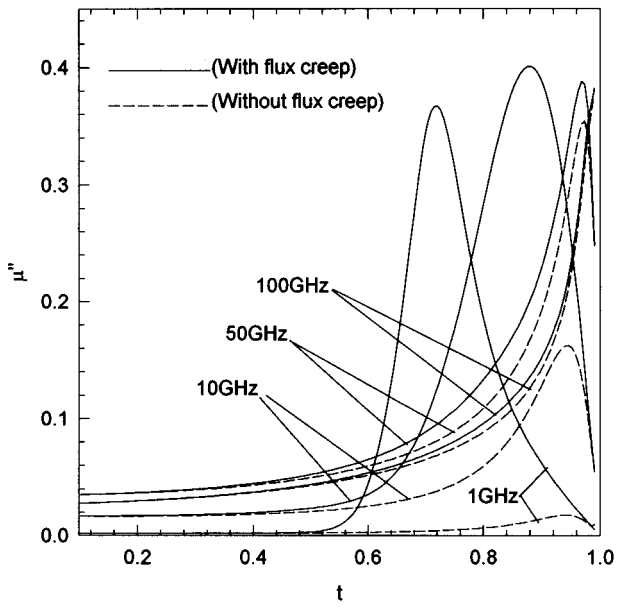

FIG. 4. Imaginary part of permeability Eq. (6) as a function of reduced temperature $t=T/T_c$ for the cases where creep is both included and excluded with fixed reduced field $b=0.01$ at various microwave frequencies. The slab thickness 5 μm and material constants are given in the text.

so that the complex penetration depth in Eq. (1) strongly relies on the frequency. The creep effect is usually modeled as a resistor in series with pinning inductors in a circuit representation. At a frequency well below f_c, the vortices can move freely with modified viscosity $\eta+(k_p/\omega_c)$, instead of η only.[42] The crossover frequency as a function of reduced temperature is shown in Fig. 5, where another characteristic frequency $f_0=\omega_0/2\pi$ is also given. The maximum f_c is

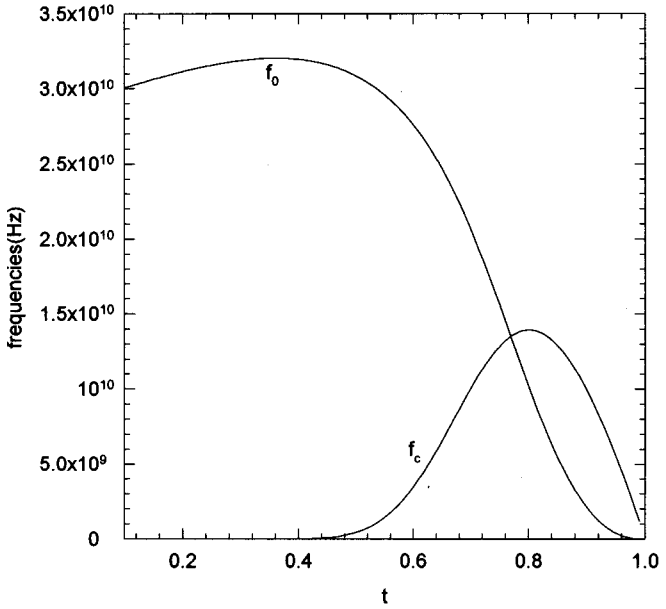

FIG. 5. Temperature-dependent characteristic frequencies ω_c and ω_0 when the creep is considered. Here $\omega_0=(\kappa_p/\eta)\, I_1(\nu)/I_0(\nu)$ and $\omega_c=\omega_0/[I_0^2(\nu)-1]^{1/2}$ with $\nu=U_0(B_0,T)/2k_BT$. Material parameters are given in the text.

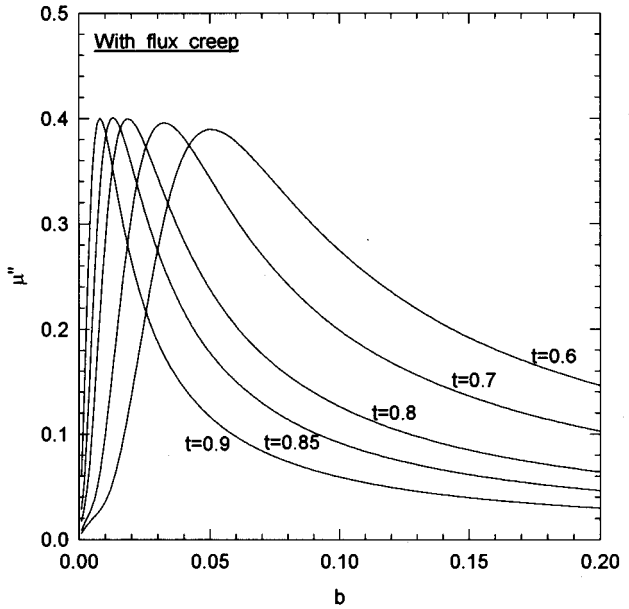

FIG. 6. Plot of μ'' of slab with $\tilde{\lambda}$ given in Eq. (1) vs reduced field $b\equiv B_0/B_{c_2}(0)$ at $f=10$ GHz for different reduced temperatures $t\equiv T/T_c=0.6$, 0.7, 0.8, 0.85, and 0.9. The slab thickness is 5 μm and the material parameters used are given in the text.

about 14 GHz. For frequencies $f_c<f\leq f_0$, the vortex dynamics is dominated by flux pinning; $\tilde{\lambda}$ is then independent of frequency. If the frequency is $f>f_0$, the vortices are not pinned at all, and the dissipation is consequently due to free viscous motion. Finally, the peak temperature in Fig. 4 increases with increasing frequency. Moreover, the peak eventually disappears at 100 GHz. In Fig. 6, we show μ'' as a function of reduced static field at different temperatures. The peak is broadened more as the temperature decreases; however, the peak height changes appreciably. The reduced field at the μ'' peak increases with decreasing temperature.

We now turn our attention to anisotropic superconductors. As an instructive illustration, we again investigate the flux-flow regime so that $\tilde{\lambda}_a\rightarrow(1+i)\,\delta_{fx}/2$ and $\tilde{\lambda}_c\rightarrow(1+i)\,\delta_{fy}/2$. For convenience, we define $x\equiv c/\delta_{fx}$ and $y\equiv a/\delta_{fy}$; then, the permeability in Eq. (27) of an anisotropic rod can be expressed as

$$\mu=\sum_{n=0}^{\infty}\frac{2}{q_n^2}\left[\frac{\tanh[\sqrt{q_n^2(x^2/y^2)-2ix^2}]}{\sqrt{q_n^2(x^2/y^2)-2ix^2}}+\frac{\tanh[\sqrt{q_n^2(y^2/x^2)-2iy^2}]}{\sqrt{q_n^2(y^2/x^2)-2iy^2}}\right]. \tag{31}$$

In the case of $y\rightarrow\infty$ $(a\rightarrow\infty)$, the result reduces to that of a slab described in Eq. (28) and has a dissipation peak (0.417) at $x=c/\delta_{fx}=1.13$. Equation (31) has a minimum peak when $x=y$. The condition $x=y$ reveals that the rod is equivalently a square one, but not actually a square rod in shape. In this equivalent square rod, the dissipation peak is a minimum. All the behaviors are very similar to those given in Fig. 1. Therefore, the thin edges should be dealt with carefully. Additionally, the permeability in expression (31) is quite analogous to the study of Gough and Exon.[6] They considered the normal-

state response of anisotropic superconductors in the parallel field configuration. The permeability is derived from the anisotropic magnetic flux diffusion equation. The authors pointed out the importance of thin edges on the microwave response of a platelet crystal. Our result shown in Eq. (31) can reproduce all their discussion provided that $B_0 \rightarrow B_{c_2}(T)$, the upper critical field, because as B_0 approaches $B_{c_2}(T)$, this will imply a divergent $\lambda(B_0,T)$, which in turn makes $\delta_{\rm nf} \rightarrow \delta_n = (2\rho/\mu_0\omega)^{1/2}$ and $\tilde{\lambda} \rightarrow (1+i)\delta_n/2$, a penetration depth of the normal-state response.

As for the general consideration of vortex dynamics, one can also execute similar calculations from Eq. (27). However, some care should be taken before the execution. In the parallel configuration, the vortex motion is anisotropic and consequently the material parameters such as $B_{c_2}(0)$, viscosity, and London penetration are strongly dependent on the anisotropic ratio $\gamma \equiv \lambda_c/\lambda_{ab} = \sqrt{m_c/m_{ab}}$. Besides, the field-orientation-dependent Labusch constant κ_{p0} and anisotropic normal-state resistivities should also be taken into account altogether, remembering that the parameters used previously in the analysis of the isotropic case are the in-plane ones. The c-axis parameters now are given as follows. The zero-temperature upper critical field $B_{c_2}(0) = 112\gamma$ T, normal-state resistivity[45] $\rho_c = 1.3/T + (3.2\times 10^{-5})$ T, Labusch constant[38] $\kappa_{p0} = 2.2\times 10^5$ N m^{-2}, and the activation barrier height[46] $U = 0.15\gamma$ eV T. Here the anisotropic ratio γ is reported to be 5–8 for the high-T_c superconductor YBCO.[47] With these parameters, we can investigate the ac response of anisotropic flux motion. Also, one is able to tell the different of responses between anisotropic and isotropic superconductors. The results with flux creep based on our generalized Coffey-Clem model are shown in Figs. 7–9 where the results of the isotropic one ($\gamma = 1$) are given for the purpose of comparison. Figures 7(a) and 7(b) display the dependence of μ'' on reduced temperature for two thicknesses $2c = 5$ and 10 μm of the platelet. As can be seen in Fig. 7(a), the anisotropy makes the μ'' peak more broadened and the peak temperature is lowered considerably compared with the isotropic one. What is more, the peak height is also increased appreciably. In the anisotropic ones, the peak temperature decreases with increasing the anisotropy and no appreciable change in peak height is observed. In Fig. 7(b), the inclusion of anisotropy again lowers the peak temperature, but not as large as in (a). The results indicate that the microwave response is strongly dependent on the material anisotropy and sample size. The magnetic field dependence of the microwave dissipation is shown in Fig. 8. Figure 8(a) illustrates that the anisotropy has narrowed the curve of μ'' and the peak is confined around $b = 0.01$ at $f = 10$ GHz and $t = 0.6$. As the field increases, the dissipation in the anisotropic superconductor is depressed much in comparison with the isotropic one. The same condition for a thicker platelet, $2c = 10$ μm, causes the μ'' curve to be more broadened as depicted in Fig. 8(b). Furthermore, the peak heights are decreased appreciably with increasing γ in anisotropic case in this condition. The influence of anisotropy on μ'' as functions of reduced temperature and static field appears to be quite different. One is that the curve is broadened in Fig. 7 and the other narrowed in Fig. 8. Finally, we demonstrate the frequency-dependent μ'' in Fig. 9. Apparently, the anisotropy has highly enhanced the microwave losses. Besides, the disappearance in the μ'' peak in the isotropic superconductor now emerges in the anisotropic ones as shown in Figs. 9(a) and 9(b). The effect of sample size on the μ'' peak is also observed in these two figures. The increase in thickness of the sample makes the peak shape more sharp and the peak frequency is localized near 5 GHz.

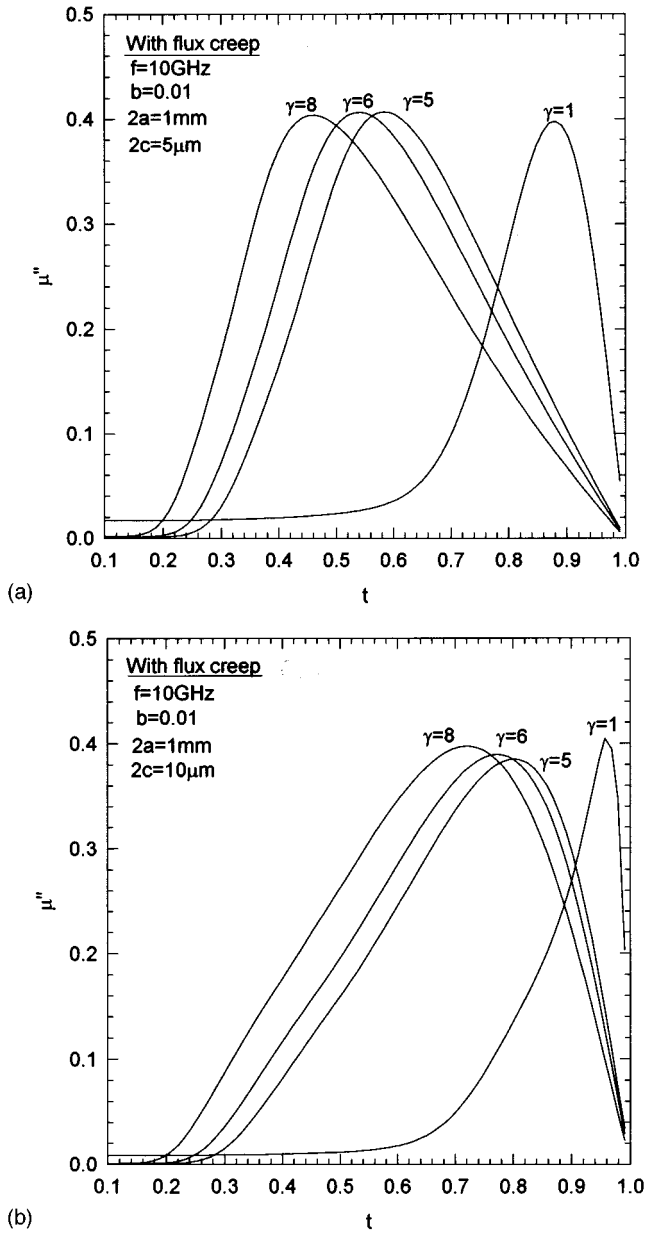

FIG. 7. (a) Plot of μ'' in Eq. (27) of a rectangular rod, $2a = 1$ mm, $2c = 5$ μm at $f = 10$ GHz and $b = 0.01$. The material parameters used are described in the text. (b) Plot of μ'' in Eq. (27) of a rectangular rod, $2a = 1$ mm, $2c = 10$ μm at $f = 10$ GHz and $b = 0.01$.

According to the Figs. 7–9, the influence of anisotropy together with sample size on the μ'' peak has been clearly elucidated so far. The results suggest the importance of anisotropy in the analysis of the microwave response of high-temperature superconducting platelet crystals in the parallel field configuration.

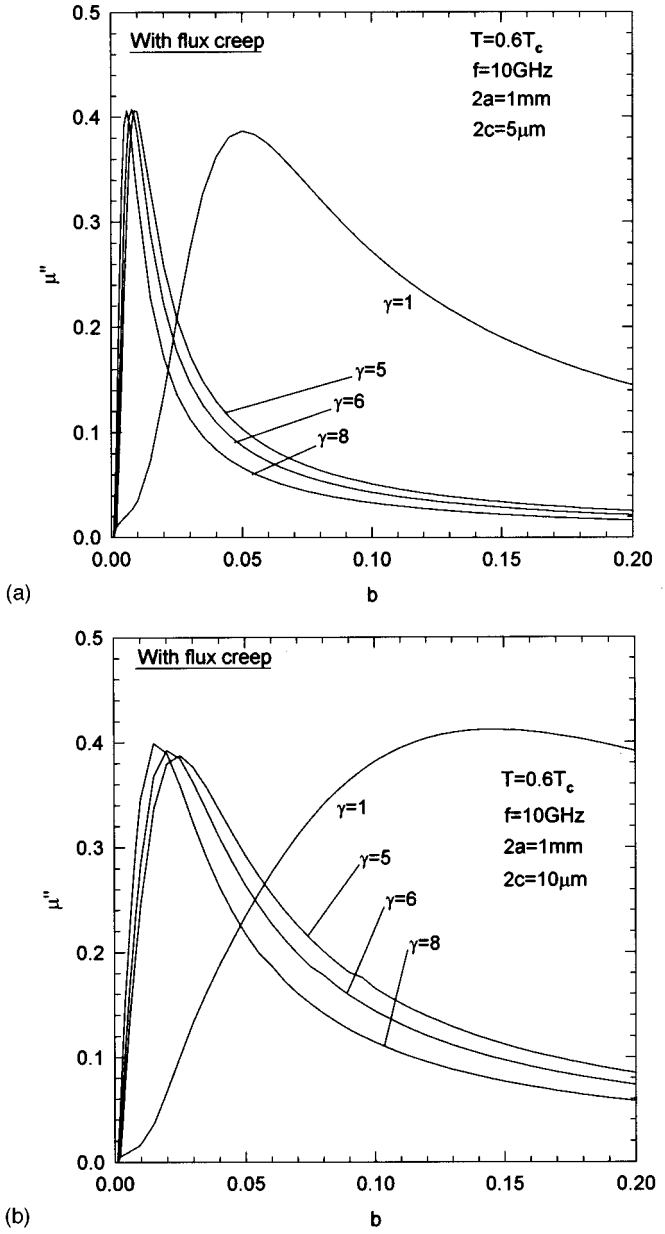

FIG. 8. (a) Field-dependent imaginary part of μ in Eq. (27) of a rectangular rod, $2a=1$ mm, $2c=5$ μm at $T=0.6T_c$ and $f=10$ GHz. (b) Field-dependent imaginary part of μ in Eq. (27) of a rectangular rod, $2a=1$ mm, $2c=10$ μm at $T=0.6T_c$ and $f=10$ GHz.

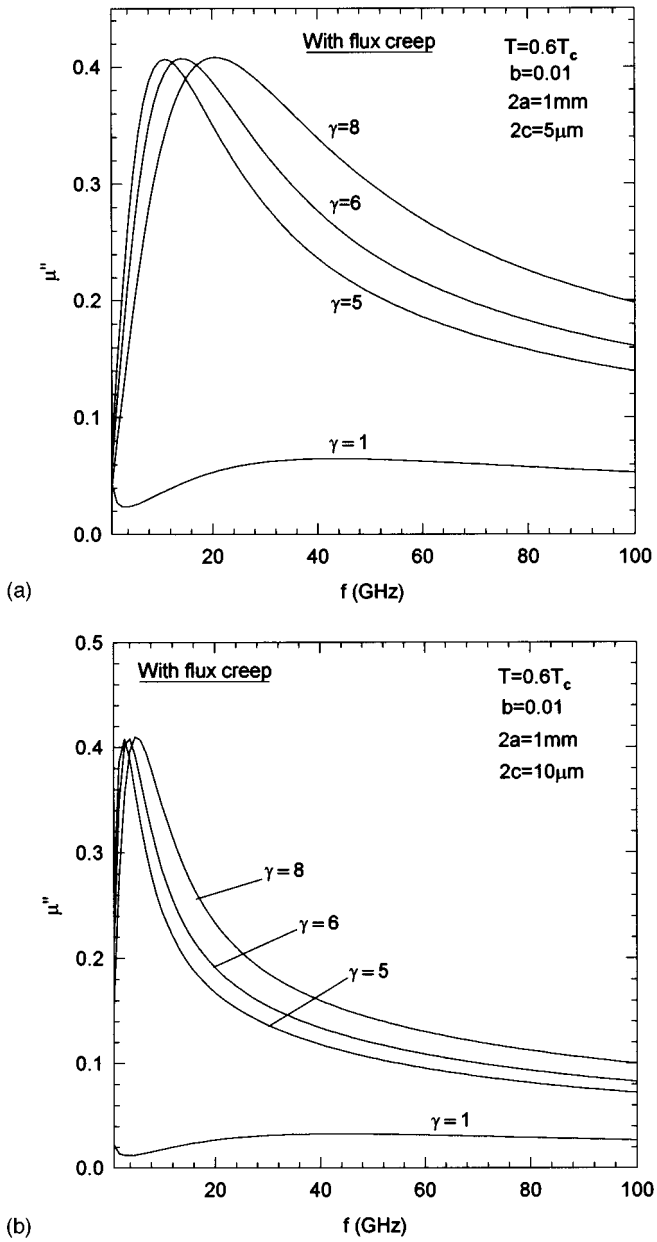

FIG. 9. (a) Frequency-dependent imaginary part of μ in Eq. (27) of a rectangular rod, $2a=1$ mm, $2c=5$ μm at $T=0.6T_c$ and $b=0.01$. (b) Frequency-dependent imaginary part of μ in Eq. (27) of a rectangular rod, $2a=1$ mm, $2c=10$ μm at $T=0.6T_c$ and $b=0.01$.

IV. SUMMARY

We have extended the Coffey-Clem model to the anisotropic case. The idea of a self-consistent treatment of vortex dynamics as well as the anisotropic London electrodynamics establish the basis for our extension. The permeability in Eq. (27) acts as a good candidate for the microwave response of anisotropic superconducting single crystals in the shape of platelets in the parallel field configuration. The permeability depends on the anisotropic complex penetration depths, which are determined by a self-consistent treatment of vortex dynamics. Our results in Eqs. (23) and (25) provide some conversion relations from isotropic to anisotropic superconductors within the framework of the Coffey-Clem model. Besides, our derivations provide a possible tool for experimentally determining the anisotropic properties such as viscosity, Labusch constant, normal-fluid resistivity, and so forth.

Numerical studies indicate some fundamental information about the vortex response to a microwave field. If the vortex dynamics is dominated by flux flow, then the response behaves as a resistive one. Accordingly, the microwave properties of platelike single crystals are highly related to the thin edges of samples for both isotropic and anisotropic superconductors because of the skin size effect. A square rod in the isotropic case or an equivalent square rod in anisotropic superconductors gives the possible minimum peak height and the highest peak frequency. Therefore, one can prepare suitable sample dimensions to get the minimum peak and in

turn the anisotropic viscosity is able to be extracted. For material parameters on the order of high-temperature superconductors, the YBCO system, the inclusion of flux creep effectively enhances the dissipation heavily and makes the peak height essentially unchanged at various static magnetic fields. The dependence of vortex dynamics on microwave frequency is also numerically illustrated to indicate the fact that the creep is detected at the low-frequency regime. At very high frequency, the dissipation peak becomes very sharp and moves closely to T_c; eventually the peak shape vanishes. Our results specifically indicate the effects of thin edges of plates should be noted in the microwave study. To obtain the dissipation peak, it is indicated that a thin platelet would be in preference to a thick platelet. Also, the consideration of anisotropy makes the microwave properties of the anisotropic quite different from those of the isotropic superconductors. It therefore reveals that the microwave response is strongly dependent on the anisotropic vortex motion together with the sample dimension.

The generality here encompasses all the isotropic results given by Coffey and Clem[31] previously and the special consideration such as the anisotropic normal-state response provided by Gough and Exon.[6] The extension also provides the possibility of studying highly anisotropic high-T_c superconductors, the BSCCO system. In BSCCO, the creep is more pronounced because of its relatively low activation energy. Regarding the interpretation, the irreversibility line in the mixed state, the extension here gives more possible dependence on sample geometry, too.

ACKNOWLEDGMENT

The work is supported by the National Scientific Council through Grant No. NSC85-2112-M009-037.

[1] P. L. Gammel, L. F. Schneemeyer, J. V. Waszczak, and D. J. Bishop, Phys. Rev. Lett. **61**, 1666 (1988).
[2] S. de Brion, R. Calemczuk, and J. Y. Henery, Physica C **178**, 225 (1991).
[3] G. D'Anna, W. Benoit, W. Sadowski, and E. Walker, Europhys. Lett. **20**, 167 (1992).
[4] Ph. Seng, R. Gross, U. Baier, M. Rupp, D. Koelle, R. P. Huebener, P. Schmitt, G. Saemann-Ischenko, and L. Schultz, Physica C **192**, 403 (1992).
[5] S. Revenaz, D. E. Oates, D. Labbe-Lavigne, G. Dresselhaus, and M. S. Dresselhaus, Phys. Rev. B **50**, 1178 (1994).
[6] C. E. Gouch and N. J. Exon, Phys. Rev. B **50**, 488 (1994).
[7] J. Owliaei, S. Sridhar, and J. Talvacchio, Phys. Rev. Lett. **69**, 3366 (1992).
[8] M. S. Pambianchi, D. H. Wu, L. Ganapathi, and S. Anlage, IEEE Trans. Appl. Supercond. **AS-3**, 2774 (1993).
[9] C. P. Bean, Rev. Mod. Phys. **2**, 31 (1964).
[10] J. I. Gittleman and B. Rosenblum, Phys. Rev. Lett. **16**, 734 (1966).
[11] A. M. Campbell, J. Phys. C **2**, 1492 (1969); **4**, 3186 (1971).
[12] C. J. van der Beek, V. B. Geshkenbein, and V. M. Vinokur, Phys. Rev. B **48**, 3393 (1993).
[13] E. H. Brandt, Z. Phys. B **80**, 167 (1990).
[14] P. H. Kes, J. Aarts, J. van den Berg, C. J. van der Beek, and J. A. Mydosh, Supercond. Sci. Technol. **1**, 242 (1989).
[15] V. B. Geshkenbein, V. M. Vinokur, and R. Fehrenbacher, Phys. Rev. B **43**, 3748 (1991).
[16] M. W. Johnson, D. H. Douglass, and M. F. Bocko, Phys. Rev. B **44**, 7726 (1991).
[17] L. Ji, R. H. Sohn, G. C. Spalding, C. J. Lobb, and M. Tinkham, Phys. Rev. B **40**, 10 936 (1989).
[18] Y. B. Kim, M. J. Stephen, and W. F. Vinen, in *Superconductivity*, edited by R. D. Park (Dekker, New York, 1969), Vol. 2.
[19] C. J. van der Beek and P. H. Kes, Phys. Rev. B **43**, 13 032 (1991).
[20] N. C. Yeh, Phys. Rev. B **43**, 523 (1991).
[21] A. E. Koshelev and V. M. Vinokur, Physica C **173**, 465 (1991).
[22] A. I. Larkin and Yu. N. Ovchinnicov, J. Low Temp. Phys. **43**, 409 (1979).
[23] M. V. Feigel'man and V. M. Vinokur, Phys. Rev. B **41**, 8986 (1990).
[24] L. W. Chen and M. C. Marchetti, Phys. Rev. B **50**, 6382 (1994).
[25] M. C. Marchetti and D. R. Nelson, Physica C **174**, 40 (1991).
[26] E. B. Sonin, A. K. Tagantsev, and K. B. Traito, Phys. Rev. B **46**, 5830 (1992).
[27] E. B. Sonin and K. B. Traito, Phys. Rev. B **50**, 13 547 (1994).
[28] E. H. Brandt, Phys. Rev. Lett. **67**, 2219 (1991).
[29] M. W. Coffey and J. R. Clem, Phys. Rev. Lett. **67**, 386 (1991).
[30] M. W. Coffey and J. R. Clem, IEEE Trans. Magn. **MAG-27**, 2136 (1991).
[31] M. W. Coffey and J. R. Clem, Phys. Rev. B **45**, 9872 (1992).
[32] M. W. Coffey and J. R. Clem, Phys. Rev. B **45**, 10 527 (1992).
[33] M. W. Coffey and J. R. Clem, Phys. Rev. B **46**, 11 757 (1992).
[34] J. R. Clem and M. W. Coffey, J. Supercond. **5**, 313 (1992).
[35] T. Hanaguri, Y. Iino, A. Maeda, N. Motohira, and K. Kishio, Physica C **235**, 1991 (1994).
[36] T. Shibauchi, H. Kitano, K. Uchinokura, A. Maeda, T. Kimura, and K. Kishio, Phys. Rev. Lett. **72**, 2263 (1994).
[37] K. Zhang, D. A. Bonn, S. Kamal, Ruixing Liang, D. J. Baar, W. N. Hardy, D. Basov, and T. Timusk, Phys. Rev. Lett. **73**, 2484 (1994).
[38] D. H. Wu and S. Sridhar, Phys. Rev. Lett. **65**, 2074 (1990).
[39] Z. Hao and J. R. Clem, IEEE Trans. Magn. **MAG-27**, 1086 (1991).
[40] A. M. Campbell and J. E. Evetts, *Critical Currents in Superconductors* (Barnes & Noble, New York, 1972).
[41] W. Tomasch *et al.*, Phys. Rev. B **37**, 9864 (1988).
[42] A. M. Portis, *Electrodynamics of High-Temperature Superconductors* (World Scientific, Singapore, 1993), Chap. 9.
[43] T. P. Orlando and K. A. Delin, *Foundations of Applied Superconductivity* (Addison-Wesley, Reading, MA, 1991).
[44] C. J. Wu and T. Y. Tseng, Phys. Rev. B **54**, 488 (1996).
[45] T. Penney, S. von Molnar, D. Kaiser, F. Holtzberg, and A. W. Kleinsasser, Phys. Rev. B **38**, 2918 (1988).
[46] A. Freimuth, in *Frontiers in Solid State Science*, edited by L. C. Gupta and M. S. Multani (World Scientific, Singapore, 1993), Vol. 1.
[47] G. J. Dolan, F. Holtzberg, C. Feild, and T. R. Dinger, Phys. Rev. Lett. **62**, 2184 (1989).